Journal of Hazardous Materials 172 (2009) 1175–1184

Contents lists available at ScienceDirect

Journal of Hazardous Materials

journal homepage: www.elsevier.com/locate/jhazmat

Properties of iron-based mesoporous silica for the CWPO of phenol: A comparison between impregnation and co-condensation routes

L. Xiang[a,b], S. Royer[b], H. Zhang[a], J.-M. Tatibouët[b], J. Barrault[b], S. Valange[b,*]

[a] Department of Environmental Engineering, Wuhan University, P.O. Box C319, Luoyu Road, 129#, Wuhan 430079, PR China
[b] LACCO, Université de Poitiers-CNRS, ESIP, 40 avenue du Recteur Pineau, F-86022 Poitiers Cedex, France

ARTICLE INFO

Article history:
Received 6 May 2009
Received in revised form 28 July 2009
Accepted 28 July 2009
Available online 4 August 2009

Keywords:
Fe-SBA15
CWPO
Phenol
Fenton

ABSTRACT

Iron-based mesoporous silica materials were prepared according to different impregnation and co-condensation procedures. Several complementary techniques, including XRD, TEM/EDX and nitrogen sorption isotherms were used to evaluate the final structural and textural properties of the calcined Fe/SBA-15 materials. While Fe_2O_3 isolated particles of which the size is close to the silica pore diameter (~7–8 nm) were obtained using classical wet impregnation procedure, smaller iron oxide particles (~2–4 nm) homogeneously dispersed within the hexagonal pore structure of the SBA15 host support were generated by self-combustion of an impregnated iron-glycinic complex. By contrast, the various co-condensation routes used in this work were less efficient to generate iron oxide nanoparticles inside the silica mesopores. Catalytic performances of the materials were evaluated in the case of total phenol oxidation by H_2O_2 in aqueous solution at ambient conditions. Large differences in terms of catalytic activity and iron species stability were observed. While the impregnated solids proved to be the most active catalysts (highest Fe_2O_3 nanoparticles dispersion), iron leaching was observed in aqueous solution, accounting for a homogeneous catalytic contribution. In contrast, the co-condensed samples exhibiting larger iron oxide clusters stabilized over the silica surface proved more efficient as active sites in Fenton catalysis.

1. Introduction

Industrial processes generate a wide variety of wastewaters containing organic pollutants with negative impact for ecosystems. In accordance with the increasingly stringent environmental legislation, the effective pollutants degradation or removal is a challenging task implying the development of advanced and economic viable oxidation processes (AOPs) [1–12]. One of the most promising AOPs is based on the use of the Fenton reagent ($H_2O_2 + Fe^{2+}$) commonly carried out in homogeneous phase. Catalytic wet hydrogen peroxide oxidation (CWHPO) allows performing oxidation of organic pollutants in ambient conditions, thanks to the redox properties of metallic cations used to generate reactive hydroxyl radicals. However, in order to overcome the major drawbacks of the homogeneous system (iron removal, etc.), heterogeneous Fenton-type systems have been prepared to catalyze the oxidation of various organic compounds in mild reaction conditions.

Immobilization of transition metal ions, mainly iron and copper, over different supports, such as zeolites [13–21], nafion [22], alumina [23–25], carbon [26–28], ion-exchange resin [29], alginate gel beads [30], clays [31–37] or perovskites [38–40] has been described in the literature for application in CWHPO processes. The catalytic activity of these materials, as well as their stability, is strongly related to the dispersion of the active phase and the interaction between the active centers and the support. Recently, interesting results on the CWPO process and photo-assisted Fenton degradation of phenolic solutions were obtained in the presence of iron-supported mesostructured silica supports [41–46].

In this work, iron-based mesoporous SBA-15 type silica materials were synthesized by using a single or two steps procedure, namely by co-condensation of iron and silica precursors or by classical wet impregnation of iron precursor on calcined mesoporous SBA-15 host support, following literature as well as original home-made syntheses procedures. Various characterization techniques, such as X-ray diffraction, nitrogen sorption isotherms and transmission electronic microscopy coupled to EDX analyses were used to evaluate the final structural and textural properties of the calcined mesostructured Fe_2O_3/SiO_2 materials, as well as the dispersion of the iron species in both samples series. The catalytic performances of the impregnated and co-condensed iron-based silica materials were determined in total phenol oxidation using hydrogen peroxide in ambient conditions (atmospheric pressure and temperature close to the ambient). Our aim consisted in investigating the influence of the synthesis procedure on the phenol

* Corresponding author. Tel.: +33 5 49454048; fax: +33 5 49453349.
E-mail address: sabine.valange@univ-poitiers.fr (S. Valange).

0304-3894/$ – see front matter © 2009 Elsevier B.V. All rights reserved.
doi:10.1016/j.jhazmat.2009.07.121

elimination activity and total organic carbon (TOC) abatement level, as well as on the iron particles size and dispersion. The stability of both the iron active species and the silica support during the catalytic reaction was also evaluated.

2. Materials and methods

2.1. Catalysts preparation

Pure siliceous mesoporous SBA-15 was prepared using classical literature procedures using Pluronic P123 and tetraethylorthosilicate (TEOS) as surfactant and silica source respectively, at 38 °C for 24 h. The resulting mixture was transferred to Teflon bottles and heated at 130 °C for 24 h. The white solid was filtered, washed with distilled water, air-dried at 80 °C for 12 h and calcined at 600 °C for 5 h under flowing air (heating ramp of 1 °C min^{-1}). The Fe/SBA-15 materials were prepared by using different impregnation and co-condensation procedures. In each case, the amount of iron precursor was adjusted to obtain a final Fe_2O_3 content of 10 wt% after calcination.

2.1.1. Impregnated samples

Two samples, labeled SBA15-iFe(NO_3) and SBA15-acFe(NO_3), were respectively prepared by classical wet impregnation of the silica support by iron nitrate or by self-combustion of an iron-glycinic complex within the silica porosity [47,48]. For sample SBA15-iFe(NO_3), the mixture "iron nitrate solution and SBA-15 silica" was slowly evaporated at 50 °C, then the impregnated solid was dried in air at 110 °C for 12 h, before being calcined at 600 °C for 5 h (heating rate of 1 °C min^{-1}). The synthesis of sample SBA15-acFe(NO_3) proceeded in three successive steps: (1) complexation of the iron nitrate precursor with glycine; (2) impregnation of calcined SBA-15 silica with the complex; (3) self-combustion of the iron-glycinic complex. Glycine was added to a solution of iron nitrate and the mixture stirred for 2 h. 0.9 g of freshly calcined SBA15 was slowly added to this solution and the temperature was increased to 110 °C. When a dry powder was obtained, the solid was transferred in a furnace for glycine ignition (280 °C) followed by a calcination step at 600 °C in order to eliminate the remaining carbonaceous residues coming from incomplete glycine combustion.

2.1.2. Co-condensed samples

This procedure consisted in the addition of an iron precursor (iron nitrate or chloride) during the acidic SBA-15 silica synthesis. Three samples, labeled SBA15-coFe(NO_3), SBA15-coFeCl and SBA-REF, were prepared according to the procedure used for the SBA15 silica except that iron precursor was added to the synthesis media and precipitated with ammonia at pH 3.5. The co-condensed solids were then hydrothermally treated at 100 °C (SBA-REF [41,44,46]) or 130 °C (SBA15-coFe(NO_3) and SBA15-coFeCl).

Briefly, 8 g of triblock copolymer P123 was dissolved in 250 mL HCl 1.9 mol L^{-1} and the solution stirred at 35 °C for 2 h, before the addition of iron precursor ($Fe(NO_3)_3$, $9H_2O$ or $FeCl_3{\cdot}6H_2O$). Then 15.5 mL of TEOS was slowly added to the solution under stirring and the pH increased to 3.5 by ammonia addition (35 wt%). The precipitate was maintained at 38 °C for 24 h, before being transferred in an autoclave and heated at 130 °C for 24 h. The red solid was filtered, washed with distilled water, air-dried at 80 °C for 12 h and calcined at 600 °C for 5 h under flowing air.

2.2. Catalysts characterization

Powder small- and wide-angle XRD patterns of the calcined Fe/SBA-15 samples were recorded on a Bruker AXS D5005 diffractometer equipped with monochromatized Cu Kα radiation (λ = 1.5418 Å) at 40 kV, 30 mA. Phase identification was performed by comparison with the information of the JCPDS database. Iron chemical analysis was achieved by Atomic Emission Spectroscopy with Induced Coupled Plasma (ICP-AES) using a Varian Vista AX system. The surface area and pore size analysis of the samples were carried out by adsorption–desorption of nitrogen on a Micromeritics ASAP 2010 instrument (−196 °C). Prior to N_2 adsorption, the samples were degassed under vacuum at 250 °C for at least 6 h. The surface of the Fe/SBA-15 samples, as well as the iron oxide particle size analysis, were investigated by TEM (Philips CM120 microscope operated at 120 kV) coupled to an EDX analyzer (fixed probe) for Fe spot detection over the sample surface. Electron microdiffraction patterns were also recorded to identify the nature of the iron-bearing particles. The samples were at first included in a resin that was cut into sections of 30–50 nm with a microtome equipped with a diamond cutter, before they were supported on a carbon-coated gold grid.

2.3. Catalytic wet peroxide oxidation of phenol

Catalytic tests were performed in ambient conditions (at atmospheric pressure and at 25 or 40 °C) in a thermostated semi-batch pyrex reactor of 250 mL (Fig. 1) using phenol as reactant and hydrogen peroxide as oxidant. The reactor was equipped with a pH electrode to continuously monitor the pH value of the reaction solution. The reaction pH value was maintained by addition of small amounts of diluted H_2SO_4 solution (0.1 mol L^{-1}), close to its optimum value (pH ≈ 3.7) under continuous stirring. The catalyst (100 mg) was put into 100 ml of an aqueous phenol solution (5×10^{-4} mol L^{-1}) under continuous stirring, 15 min before the beginning of the hydrogen peroxide addition. H_2O_2 solution (0.1 mol L^{-1}) was added continuously to the phenol solution containing the catalyst at a constant flow rate of 2 mL h^{-1} through a dosimeter (Dosimat 725 Metrohm). The reaction was performed under air flow (2 L h^{-1}) bubbling directly through the reaction solution in order to maintain the amount of dissolved oxygen close to its saturation concentration. After 4 h of reaction, the excess of hydrogen peroxide with respect to the required amount needed for a complete phenol oxidation (according to the reaction: $C_6H_5OH + 14H_2O_2 \rightarrow 6CO_2 + 17H_2O$) was only 1.14.

Phenol conversion as well as the products formed by the reaction were determined during the overall reaction (4 h) using a high performance liquid chromatography (Waters HPLC) equipped with an Aminex HPX-87 (Biorad) column. The Total Organic Carbon (TOC) content was measured by a DC-190 Dohrmann TOC meter. Iron leaching was systematically evaluated by ICP analyses after catalytic tests.

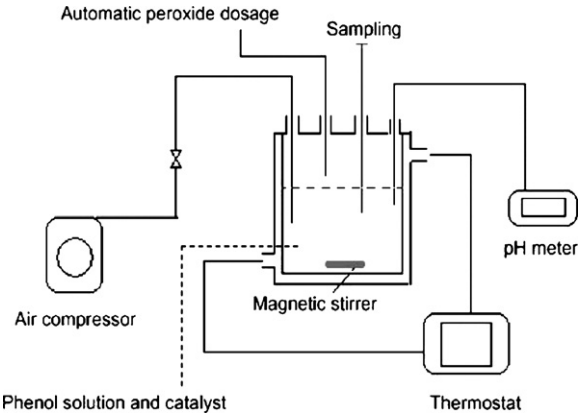

Fig. 1. Schematic view of the semi-batch type reactor system used for the CWPO reaction.

Table 1
Physico-chemical properties of the calcined SBA-15 silica host support and the Fe-based impregnated and co-condensed silica samples.

Sample	Fe_2O_3 content (wt%)	Fe cont. (wt%)	S_{BET} ($m^2\ g^{-1}$)	D_{BJH} (nm)	V_{meso} ($cm^3\ g^{-1}$)	dV_{meso}[a] (%)	d_{100} (nm)	a_0 (nm)
SBA	0.0	0.0	535	7.2	1.03	–	9.20	10.6
SBA-iFe(NO_3)	10.1	7.07	406	6.8	0.63	−39	9.29	10.7
SBA-acFe(NO_3)	10.2	7.14	417	6.7	0.70	−32	9.60	11.1
SBA-coFe(NO_3)	8.4	5.87	461	8.5	1.37	+33	10.04	11.6
SBA-coFeCl	8.4	5.87	561	8.9	1.42	+38	9.92	11.5
SBA-REF	8.5	5.95	647	6.9	1.01	−2	9.60	11.1

[a] dV_{meso} being the fraction of pore volume lost after impregnation.

3. Results and discussion

Before characterizing the structural, textural and morphological properties of the Fe/SBA-15 materials prepared by various impregnation and co-condensation routes, we first checked that the iron content of the samples (expressed in terms of Fe_2O_3 wt%) remains close to the desired value. With respect to previous studies describing the preparation and catalytic properties of a Fe_2O_3/SBA-15 nanocomposite with a bulk iron content as high as 16 wt% [41,44,46], the Fe content was reduced in our case with the aim of better controlling the iron dispersion inside the impregnated and co-condensed samples. By decreasing the iron content, it is expected a lower amount of large Fe_2O_3 aggregates located on the external surface of the silica grains and an increased proportion of Fe_2O_3 particles embedded into the mesostructured silica matrix, as well as Fe^{3+} ionic species dispersed within the SBA-15 structure.

Results presented in Table 1 show that the Fe_2O_3 content of the impregnated samples (SBA-iFe(NO_3) and SBA-acFe(NO_3)) are similar and agree with the theoretical value, whereas it remains systematically lower than the desired value for the materials synthesized by co-condensation (~8.4 wt% Fe_2O_3). These data clearly indicate that the incorporation of Fe^{3+} cations during the silica synthesis is not complete under the pH conditions used (*i.e.* pH 3.5). Consequently, only ~85% of the iron species precipitated with the siliceous species during the aging step.

3.1. Samples pore structure

Small-angle X-ray diffraction patterns obtained for the different samples are presented in Fig. 2A. The SBA-15 silica as well as the two impregnated samples display well-resolved XRD lines, confirming that the hexagonal ordering in the SBA-15 silica was retained after the impregnation/calcination steps. The $d_{(100)}$ distances determined from the XRD patterns, as well as the a_0 unit cell values assuming a hexagonal structure, are summarized in Table 1. Cell parameter values ranging from 10.7 nm (SBA-iFe(NO_3) sample) to 11.1 nm (SBA-acFe(NO_3) sample) are obtained, which are close to that of the parent silica support (a_0 = 10.6 nm for SBA). This indicates that the impregnating iron precursor and its further decomposition into iron oxide by calcination (case of SBA-iFe(NO_3)) or by self-combustion (case of SBA-acFe(NO_3)) do not resulted in any drastic change in the final samples pore structure.

By contrast, for the co-condensed samples, while a well-resolved XRD pattern is obtained for the SBA-REF sample, the two other solids (SBA-coFe(NO_3) and SBA-coFeCl) display poorly defined XRD lines (Fig. 2A). Indeed, the (1 1 0) and (2 0 0) reflections of these latter compounds are rather broad, suggesting that the SBA-coFe(NO_3) and SBA-coFeCl samples exhibit a lower long range order of the pore structure or have a slightly deformed hexagonal structure. Note that for the co-condensed samples, a shift of the (1 0 0) reflection to lower 2θ values is observed, leading to slightly higher cell parameters (Table 1).

3.2. Structure of the iron-bearing particles

Wide-angle X-ray diffractograms of the samples prepared by impregnation of iron nitrate and by self-combustion of the iron-glycinic complex were recorded in the 10°–70° 2θ range (Fig. 2B). Besides the broad peak at $2\theta \sim 23°$ typical of the amorphous silica, the XRD pattern of the impregnated SBA-iFe(NO_3) sample also displays weak and broad lines at $2\theta \sim 33°$ and ~35.5°, readily attributed to α-Fe_2O_3 hematite (JCPDS file no. 089-0597) and suggesting that the size of the particles formed are large enough to be detected by XRD ($d_{crystal}$ > 3 nm). Nevertheless, the diffraction peaks intensity remains low and the large FWHM suggests that small iron particles are present and possibly located inside the silica porosity. In contrast, no discernable iron oxide reflections are visible on the diffractogram of the sample prepared by self-combustion

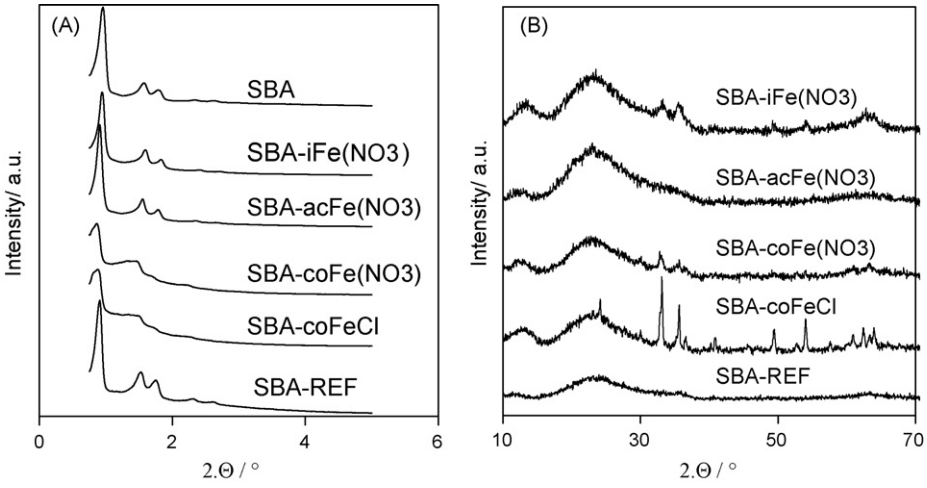

Fig. 2. Small-angle (A) and wide-angle X-ray diffraction patterns (B) of the parent SBA-15 silica sample and the impregnated and co-condensed iron-based mesoporous silica materials.

SBA-acFe(NO_3), suggesting the exclusive presence of very small nanometric Fe(III) oxidic particles that cause the classical line broadening on the XRD pattern. This observation is consistent with recent results obtained for the synthesis of supported mixed-oxide HMS-type silica materials using the same synthesis procedure [48].

Wide-angle XRD patterns of the three co-condensed samples are also presented in Fig. 2B. SBA-REF sample exhibits only the broad diffraction peak characteristics of amorphous silica and additional signals related to the iron oxide phase are hardly detectable. That result suggests, as for the SBA-acFe(NO_3) sample, that the iron phase is well dispersed within the silica mesopores or is isomorphously substituted in the silica structure. Slightly differences are observed on the XRD diagram of the sample prepared by co-condensation of iron nitrate and TEOS, since weak and broad diffraction lines attributed to the hematite phase are visible. Again, the XRD intensity remains low and the FWHM high, suggesting as in the case of the impregnated SBA-iFe(NO_3) sample that small iron particles are present inside or at the surface of the mesoporous silica. However, the sample prepared using iron chloride as Fe_2O_3 precursor (SBA-coFeCl) displays intense, well-resolved XRD lines, attributed to the hematite structure and suggesting that relatively large particles are present. This result is not compatible with a crystallization of iron oxide particles inside the silica porosity because the pore size of the host support (Table 1) would obviously lead to a limited Fe_2O_3 particle size growth and consequently to weak and broad diffraction peaks as observed for the other Fe-based mesoporous silica materials.

3.3. Samples physico-chemical properties

Table 1 summarizes the textural properties of the parent silica host support and the impregnated and co-condensed samples. SBA-15 silica sample exhibits a specific surface area of 535 $m^2\ g^{-1}$ with high pore volume (1.03 $cm^3\ g^{-1}$) and a mean pore size, determined by applying the BJH model to the desorption branch, of 7.2 nm. Classical type IV isotherm according to the IUPAC classification, with H1-type hysteresis, characteristic of cylindrical pores, is observed on Fig. 3A. As suggested by the well- resolved small-angle XRD pattern, this confirms that the silica sample presents a well-defined hexagonal pore structure. This is also substantiated by the narrow pore size distribution presented on Fig. 3B. A decrease in both specific surface area and pore volume is logically observed after the iron precursor impregnation step, from 535 to 406–417 $m^2\ g^{-1}$ (samples SBA-iFe(NO_3) and (SBA-acFe(NO_3) respectively). This corresponds to a specific surface area decrease of 24% with respect to that of the parent silica support. A similar pore volume decrease is also observed after the impregnation procedure (32% for SBA-acFe(NO_3) sample). Such values suggest some pore blocking occurring during the crystallization of iron oxide particles inside the silica mesoporosity. Indeed, a silica structure collapse, that would obviously results in a pore volume decrease, is not likely to occur as confirmed by the presence of well-resolved XRD lines patterns after calcination of the impregnated solids (Fig. 2A). Isotherms remain unchanged and a long adsorption plateau typical of the N_2 capillary condensation in the mesopores is observed in each case (Fig. 3A).

In contrast, the textural properties of the samples prepared by co-condensation drastically differ from those obtained for the impregnated compounds. While a logical decrease in specific surface area and pore volume is observed after impregnation, two of the co-condensed samples (SBA-coFeCl and SBA-REF) exhibit a higher surface area than the parent SBA-15 silica sample (Table 1). The pore size and pore volume values of the samples are also strongly affected by this synthesis procedure. While the reference co-condensed SBA-REF sample displays pore characteristics similar to those of the silica support ($V_{meso} \sim 1\ cm^3\ g^{-1}$), the two other co-condensed samples exhibit far higher pore volumes, corresponding to an increase up to 38% with respect to that of the parent silica support. This is consistent with the increase in pore size also observed for these two last samples (pores size ranging from 8.5 to 8.9 nm, Fig. 3B). These variations of the physico-chemical properties are clearly observed on the N_2 isotherms (Fig. 3A), where a shift of the N_2 adsorption and desorption steps at higher P/P_0 is noticed (characteristic of larger pore size values) for SBA-coFe(NO_3) and SBA-coFeCl samples, compared with the SBA-REF sample whose isotherm is very similar to that of the silica sample. The shape of the isotherms of samples SBA-coFe(NO_3) and SBA-coFeCl also evidence the higher pore volume exhibited by these samples.

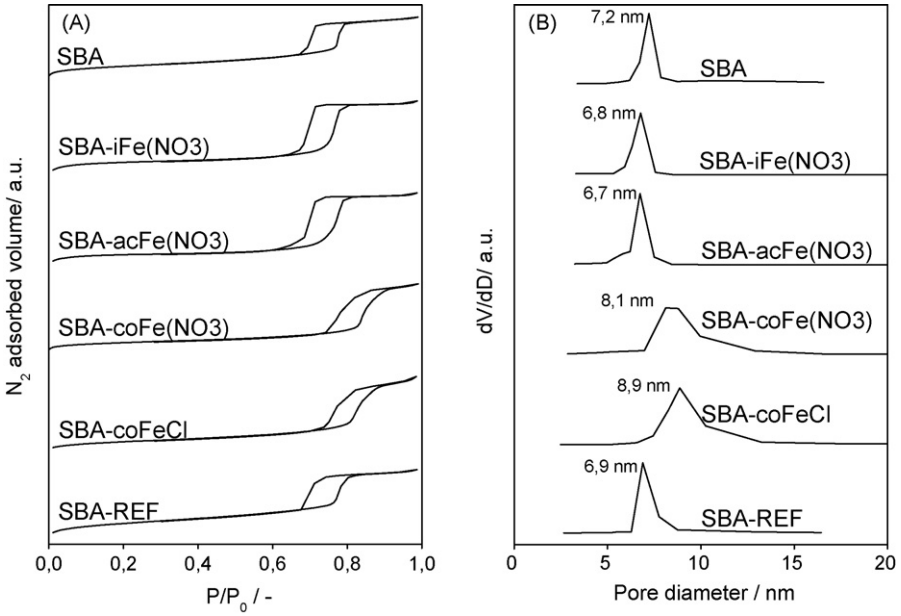

Fig. 3. N_2 adsorption–desorption isotherms (A) and the corresponding BJH pore size distributions (desorption branch) (B) obtained for the parent SBA-15 sample and for the impregnated and co-condensed samples.

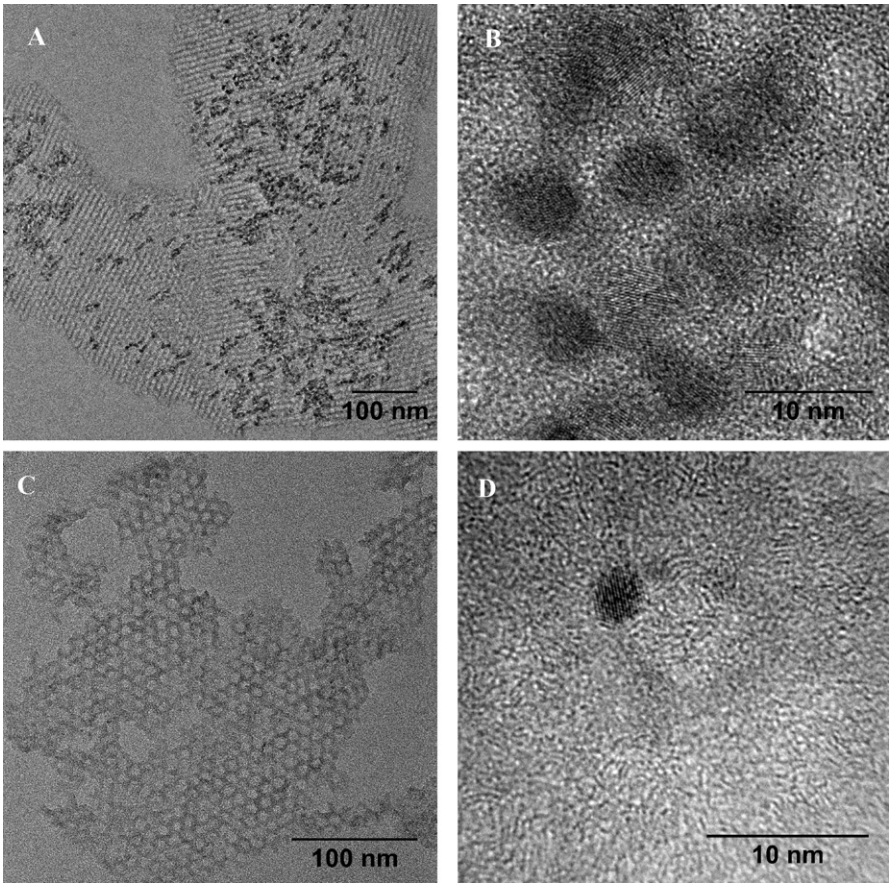

Fig. 4. Representative TEM images of the impregnated samples. SBA-iFe(NO_3) (A and B), SBA-acFe(NO_3) (C and D).

3.4. Samples morphology

Representative TEM images of the two impregnated Fe/SBA-15 samples are depicted in Fig. 4A and D and show that the silica pore structure remains unaltered after the successive impregnation-drying-calcination steps. The hexagonal pore structure arrangement is clearly visible for both impregnated samples. This observation is consistent with the XRD and N_2 sorption results that evidenced well-resolved low-angle reflections as well as typical type IV isotherm with long adsorption plateau at high P/P_0, respectively. However, differences in terms of iron oxide particles size and dispersion are observed for the two Fe/SBA-15 materials. The presence of hematite particles within the porosity of sample SBA-iFe(NO_3) is duly confirmed by TEM and electron microdiffraction analyses (Fig. 4A). Focusing on the silica mesopores (Fig. 4B) indicates the formation of "pseudo spherical" crystallized iron oxide particles of which the size is close to the silica pore diameter (~7–8 nm). For this SBA-iFe(NO_3) sample, iron oxide crystal size growth is limited by the inorganic walls of the mesoporous silica host support through a nanocasting effect.

Synthesizing iron-based mesoporous silica by self-combustion of iron nitrate with an amino acid (glycine) is shown to either prevent the iron oxide particle segregation outside the micrometric silica grains, either to generate very small Fe_2O_3 particles that are hardly detected by TEM. Only a darker contrast on the silica pore walls with respect to the pure mesoporous silica sample can be observed (Fig. 4C). These contrasts reveal the presence of crystallized Fe_2O_3 nanoparticles (Fig. 4D) which are nanometric in size (2–4 nm), meaning that the nanocasting effect occurring in SBA-iFe(NO_3) sample does not happen for SBA-acFe(NO_3) sample because the iron oxide nanoparticle size is far lower than the mean pore size of the silica. TEM observations are consistent with the conclusions deduced from XRD and N_2 sorption isotherms. Indeed, the X-ray diffraction patterns displayed the presence of the hematite phase in SBA-iFe(NO_3) sample (Fig. 2B), while no discernable iron oxide reflections were visible on the diffractogram of the SBA-acFe(NO_3) sample prepared by the self-combustion method. These observations correlate well with the observed increase in iron oxide crystal size by TEM for SBA-ac(Fe(NO_3) sample (the lowest particles size) and for SBA-iFe(NO_3) sample (particles size close to the one of the silica mesopores and, easily detected by XRD). Moreover, the nanocasting effect occurring during the synthesis/calcination of the impregnated SBA-iFe(NO_3) sample could induce some pore plugging, leading to a higher pore volume decrease than for SBA-acFe(NO_3) sample, which is confirmed by N_2 adsorption–desorption analysis (Table 1).

The size and dispersion of the iron oxide particles of the samples prepared by co-condensation strongly differ from that obtained for the impregnated samples, as observed on Fig. 5. TEM images of the sample prepared with iron nitrate as precursor (SBA-coFe(NO_3), Fig. 5A) evidence iron oxide particles of different sizes (from a few nanometers to clusters of more than 30 nm). Despite the majority of these Fe_2O_3 particles are located within the mesoporous silica matrix, a few very large Fe_2O_3 aggregates (100–200 nm) are also present on the outer surface of the silica. Nevertheless the proportion of this second Fe_2O_3 population is low by comparison with the one exhibited by the sample prepared with iron chloride as precursor (SBA-coFeCl). Besides the Fe_2O_3 particles embedded into the mesostructured matrix and the larger outer Fe_2O_3 aggregates, spot EDX analyses probing the mesostructured silica matrix also evidenced the presence of dispersed iron species within the SBA-15 structure (Fe^{3+} ionic species). TEM investigation of Fe_2O_3 particle

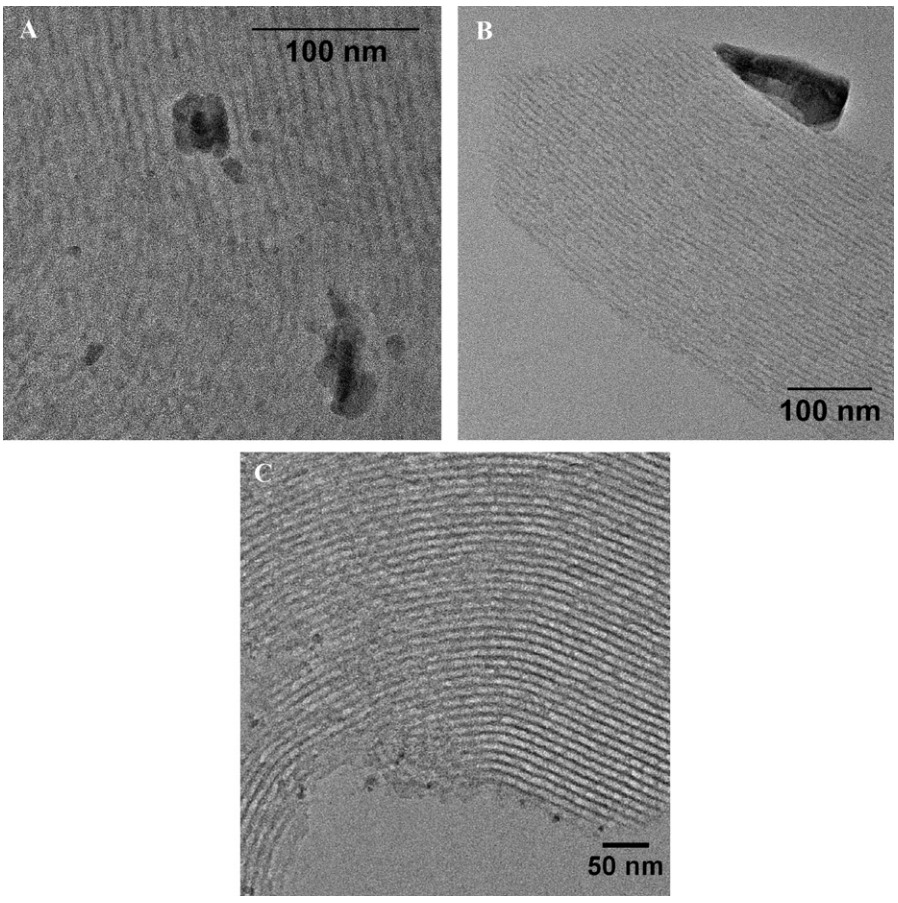

Fig. 5. Representative TEM images of the co-condensed samples. SBA-coFe(NO_3) (A), SBA-coFeCl (B), SBA-REF (C).

location in the SBA-coFeCl sample reveals hematite Fe_2O_3 large clusters coated the external surface of silica (Fig. 5B). Spot EDX probing the sample surface indicates an inhomogeneous dispersion of iron species in the silica host support, thereby confirming the low incorporation rate of iron species within the mesoporous silica matrix during synthesis. This result is also in agreement with the XRD analysis of SBA-coFeCl sample that pointed out narrow and intense reflections characteristics of hematite (Fig. 2B). Finally, small Fe_2O_3 particles having a size of less than 10 nm are detected within the mesoporous SBA-15 support of the SBA-REF sample (Fig. 5C). However part of the Fe_2O_3 was also shown to be located outside the silica grains in the form of large aggregates constituted of small iron oxide particles (figure not shown).

In light of the TEM investigations, it appears that a higher dispersion and size control of iron oxide particles are obtained for the two impregnated samples, being understood that the smallest Fe_2O_3 particles are obtained for the sample prepared by the auto-ignition route (SBA-acFe(NO_3)). Indeed, dispersed embedded hematite nanoparticles of about 2–4 nm within the mesoporous SBA-15 silica are generated by the self-combustion of iron nitrate with glycine inside the silica. Among the samples prepared by co-condensation of various iron precursors and TEOS, only SBA-coFe(NO_3) and SBA-REF compounds seem to present the iron dispersion and accessibility necessary for a use as heterogeneous catalysts.

3.5. CWPO behavior of the Fe/SBA-15 materials

The elaboration of stable and efficient heterogeneous catalysts is required for the improvement of industrial wastewater treatment processes. During the last decades, numerous heterogeneous Fenton catalysts were developed with an emphasis on the experimental synthesis conditions that are considered as key factor in the elaboration of active and stable catalysts in aqueous medium. The evaluation of the catalytic activity in phenol oxidation by H_2O_2 of the iron-based mesoporous silica prepared by impregnation and co-condensation routes was carried out at 25 and 40 °C. The catalytic reaction behavior obtained for the various Fe/SBA-15 solids is shown in Table 2 and Figs. 6 and 7.

For the impregnated series, the total phenol conversion was reached after 4 h of reaction at 25 °C, except for SBA-iFe(NO_3) sample which proved poorly active (Fig. 6). In agreement with the phenol conversion values, the lowest TOC conversion level (total mineralization of the organic matter content) is obtained for this SBA-iFe(NO_3) catalyst (6.1%), while the sample prepared by the self-combustion procedure (SBA-acFe(NO_3)) shows a TOC abatement of about 47%. This last sample exhibits a high activity in phenol conversion even at ambient temperature (25 °C), which is likely related to the presence of very small nanometric and well dispersed Fe_2O_3 particles within the silica host support. Increasing the reaction temperature up to 40 °C logically results in an increase of phenol conversion rate and TOC abatement level, up to 55% for SBA-acFe(NO_3) sample. A progressive TOC increase is observed as a function of reaction time, with stabilization at a plateau, as observed for other catalysts such as pillared clays [32]. From the results obtained for the impregnated samples, it is unambiguous that the iron oxide particles size and dispersion is of major importance to obtain high catalytic activity. The lowest iron dispersion was obtained for the sample prepared by wet impregnation of iron nitrate SBA-iFe(NO_3), that exhibits Fe_2O_3 particles of which

Table 2
Catalytic properties and stability of the different samples for the CWPO of phenol.

Sample	Results at 25 °C				Results at 40 °C			
	X (%)	TOC (%)	Fe (ppm)	% Fe	*X* (%)	TOC (%)	Fe (ppm)	% Fe
SBA-iFe(NO_3)	18.5	6.1	0.8	1.1	100	31.9	7.0	9.9
SBA-acFe(NO_3)	100	46.8	0.8	1.1	100	55.5	8.2	11.4
SBA-coFe(NO_3)	100	37.5	<0.1	0.1	100	55.4	0.1	0.1
SBA-coFeCl	100	31.4	0.1	0.2	100	46.8	0.5	0.8
SBA-REF	100	46.2	0.2	0.4	100	68.9	5.8	9.9

X and TOC: phenol and TOC conversion after 4 h of reaction; Fe: iron concentration in aqueous solution at the end the reaction; % Fe: percentage of iron leached from the catalyst at the end of the reaction.

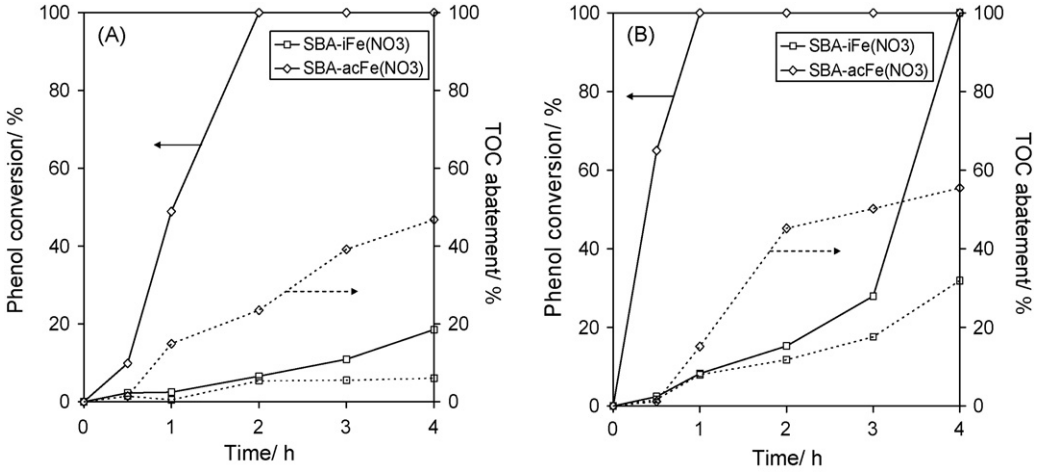

Fig. 6. Influence of the reaction temperature on the phenol conversion (full lines) and TOC abatement (dotted lines) for the impregnated samples series. 25 °C (A) and 40 °C (B).

the size is close to the silica pore diameter. One may also notice that some pore blocking, and thus a limited iron accessibility, can occur and result in a decrease of the catalytic activity. Consequently, the 7–8 nm sized iron oxide particles and the limited accessibility of these particles within the channels of the silica support are suggested to be responsible for the low catalytic activity of this sample. By contrast, the SBA-acFe(NO_3) sample synthesized by auto-ignition and containing lower Fe_2O_3 particles size, logically exhibits a higher catalytic activity.

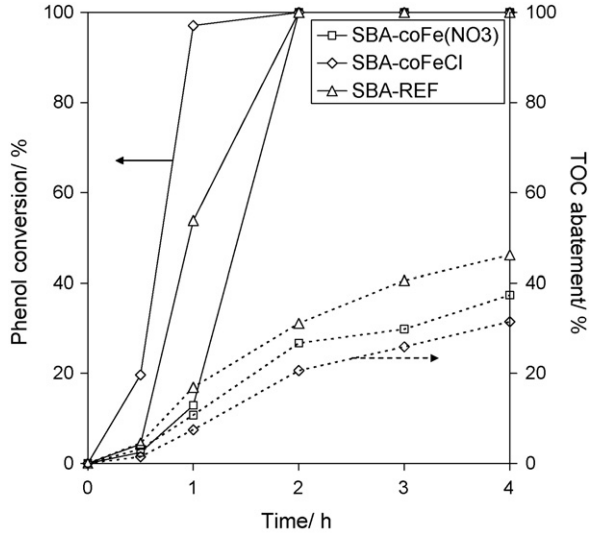

Fig. 7. Variation of the phenol conversion (full lines) and TOC abatement (dotted lines) as a function of time at 25 °C for the co-condensed samples.

The catalytic results obtained at 25 °C for the co-condensed samples are presented in Table 2 and Fig. 7. As observed for the impregnated samples, the phenol conversion readily reaches 100% for the three samples. TOC abatement values are shown to vary from 30% to 45% with similar evolutions with reaction time. Again an increase of the reaction temperature results in an increase of the TOC abatement. For instance, TOC conversion level increases from 46% at 25 °C to 69% at 40 °C for SBA-REF sample (Table 2). Whatever the reaction temperature, the catalytic activity order of the samples synthesized by the co-condensation route is the following:

SBA-REF > SBA-coFe(NO3) > SBA-coFeCl

As suggested by the results obtained for the impregnated samples, the iron oxide dispersion should also induce variation of the catalytic activity of the co-condensed samples. Indeed, the lowest iron dispersion coupled to large external hematite aggregates was reported for the SBA-coFeCl sample (Fig. 7B), resulting in the lowest phenol catalytic activity. Compared with SBA-coFe(NO_3) sample, the reference SBA-REF catalyst exhibits dispersed small Fe_2O_3 particles, that logically lead to the highest activity in the catalytic wet peroxide oxidation of phenol.

In conclusion, interesting activities for the phenol oxidation are obtained over some of the Fe-based mesoporous silica materials. The best performances are obtained for the sample prepared by direct synthesis using iron nitrate, namely SBA-coFe(NO_3), as well as the SBA-REF sample prepared by co-condensation according to the synthesis procedure described in Refs. [42–46]. This clearly shows that iron species embedded in the porosity of silica (and/or partially incorporated in the silica walls) can exhibit a high activity if their dispersion and accessibility are appropriate (*i.e.* well dispersed nanometric Fe_2O_3 particles).

For all the experiments, it should be noted that the hydrogen peroxide solution was added continuously to the phenol solution in the semi-batch slurry reactor. As already evidenced earlier [15,49], semi-batch reaction conditions (continuous addition of the hydrogen peroxide while phenol and the catalyst are introduced only at the beginning of the reaction) are preferable over batch conditions. These semi-batch conditions allow improving the efficiency of the oxidant use (selectivity in the use of H_2O_2) with respect to the competitive pathway of decomposition to H_2O and O_2. The enhancement of the hydrogen peroxide efficiency is particularly evidenced when the reaction is performed under air flow bubbling directly through the reaction solution [49,50]. This synergetic effect between the oxidant (H_2O_2) and the co-oxidant (dissolved O_2) along the reaction time appears as a pre-requisite for both the phenol and TOC conversion rates. The oxygen dissolved in water also participates in the reaction mechanism. These conditions allow avoiding the use of higher reaction temperature which would imply working at a pressure $>P_{atm}$ (to take into account the water vapor pressure in the reaction medium), thus increasing the treatment cost.

In this study, we have checked that a fraction of the added H_2O_2 remains unconverted in solution after 4 h of reaction for the sample prepared by direct synthesis with iron nitrate (SBA-coFe(NO_3)). At the end of the reaction, the excess of hydrogen peroxide with respect to the required amount needed for a complete phenol oxidation (according to the reaction: $C_6H_5OH + 14H_2O_2 \rightarrow 6CO_2 + 17H_2O$) was only 1.14. Taking into account the H_2O_2/phenol ratio used, one can deduced that the efficiency in the use of H_2O_2 is high. The phenol conversion into CO_2 is then only limited by the formation of oxalic acid in solution (major product found) whose degradation rate is low. Oxalic acid is indeed well known to be one of the most difficult chemicals to convert by CWPO.

3.6. Stability of the Fe catalysts during the Fenton reaction

Table 2 summarizes the leaching level of iron species (ppm) in the reaction medium at the end of the catalytic test (after 4 h of reaction), as well as the corresponding iron content (%) leached from the catalyst. It was first checked that the silica pore structure was not altered under the catalytic reaction conditions. The results presented in Table 2 indicate that all the catalysts exhibit excellent stability towards iron leaching at 25 °C. Indeed, very low leaching level of iron species ranging from <0.1 ppm (SBA-coFe(NO_3)) to 0.8 ppm (SBA-iFe(NO_3) and SBA-acFe(NO_3)) are observed, which indicates that the active phase is stable in the reaction medium. The most stable catalysts are the Fe/SBA-15 materials prepared by the co-condensation route. For the reference SBA-REF material, only 0.4% of the initial sample iron content is dissolved at the end of the catalytic reaction. This value is more than two times lower than the one obtained for the most stable impregnated samples SBA-iFe(NO_3) and SBA-acFe(NO_3).

Increasing the reaction temperature to 40 °C is shown to increase the concentration of Fe leached after the catalytic reaction, up to 8.2 ppm for the impregnated samples, which corresponds to 10–11% of Fe leached from the catalyst (Table 2). However, the samples prepared by co-condensation of iron nitrate or iron chloride with TEOS at 130 °C (SBA-coFe(NO_3) and SBA-coFeCl) remain stable under the experimental conditions used (Fe leached from the catalyst <1%). With the purpose to quantify the effect of dissolved iron species in the reaction medium (homogeneous catalysis), the catalytic activity is evaluated in a solution containing 2 ppm of Fe^{3+}, giving rise to a TOC conversion of 19% after 4 h of reaction at 25 °C. Consequently, the presence of soluble iron species into the reaction medium at 40 °C accounts also for a homogeneous catalytic contribution, especially for the catalysts prepared by impregnation of iron nitrate and self-combustion of the iron-glycinic complex. The low stability of these catalysts in aqueous medium when the reaction is performed at 40 °C is caused by the presence, in acidic solution, of intermediate reaction products leading to the complexation of Fe(III) ions, thus forming soluble moeities. This effect is highly pronounced for the impregnated SBA-iFe(NO_3) and SBA-acFe(NO_3) samples and the co-condensed SBA-REF catalyst, which exhibit dispersed and very small iron oxide particles, suggesting an insufficient stabilization of the Fe_2O_3 nanoparticles (weakly acidic oxide) inside the internal pore volume of the mesoporous silica (also weakly acidic oxide). As already evidenced earlier for Fe_2O_3/SBA-15 samples prepared using the chelate route [51,52], such weakly acid–acid interaction achieved between the active phase and the support resulted in moderately stable catalysts in the catalytic wet peroxide oxidation of phenol in ambient conditions. Despite well dispersed (sub)nanometric Fe_2O_3 particles were generated inside the mesopores of SBA-15 silica substrate through their incipient wetness impregnation with iron precursors of the chelate type, they proved far less resistant to leaching compared with larger Fe_2O_3 particles embedded in the mesoporous silica matrix and coupled to dispersed iron species incorporated in the silica walls, as for those samples prepared by direct synthesis ((SBA-coFe(NO_3) and SBA-coFeCl).

To prove the efficiency of a Fe/SBA-15 catalyst showing high activity and stability during the first experiment, a recycling study was performed with the SBA-coFe(NO_3) sample prepared through the co-condensation route. At the end of the first test, the catalyst was centrifuged and washed thoroughly several times, before being reintroduced inside the reactor without having been calcined. The catalytic reaction behavior (phenol conversion, TOC abatement and Fe leaching values) was shown to be totally similar during the second and third cycle of reaction, confirming the remarkable stability of the sample prepared by direct synthesis using $Fe(NO_3)_3$ as iron precursor. The concentration of leached iron species was as low as 0.1 mg L^{-1} after the third cycle of reaction, confirming that the Fe(III) active species were stabilized and strongly retained within the mesoporous silica matrix.

4. Conclusion

A series of iron-based mesoporous silica materials were prepared according to different impregnation and co-condensation routes following literature as well as home-made syntheses procedures. The structural, textural and morphological characteristics of the solids were determined before their catalytic properties in the total phenol oxidation by H_2O_2 were evaluated. Among the two synthesis routes used in this study, the wet impregnation procedure led to Fe/SBA-15 materials exhibiting a homogeneous dispersion of very small iron oxide particles within the silica porosity. While Fe_2O_3 particles with size limited by the pore diameter of the mesoporous silica (~8 nm) were obtained for the sample prepared by the classical wet impregnation procedure, very small iron oxide nanoparticles were generated within the silica mesoporosity when a more sophisticated impregnation method was used (namely self-combustion of iron-glycinic complex). The control of the size and dispersion of Fe_2O_3 particles was more difficult to achieve by using the co-condensation routes. Depending on the procedure used (iron precursor, synthesis temperature,...), small Fe_2O_3 particles as well as iron oxide clusters whose size is varying from a few nanometers to several nanometers were obtained.

The catalytic activity of the Fe/SBA-15 samples in the CWPO of phenol was strongly influenced by the iron dispersion and accessibility within or at the surface of the silica host support. The impregnated solids exhibiting the highest iron oxide dispersion

proved to be the most active catalysts, but the less stable ones in aqueous solution due to iron leaching in the reaction medium. This effect was particularly pronounced when increasing the reaction temperature from 25 to 40 °C (percentage of iron leached from the catalyst as high as 10%) and stemmed from an insufficient interaction of the Fe_2O_3 nanoparticles with the weakly acidic mesoporous silica internal pore volume. Therefore, without sufficient stabilization of nanometric and very active Fe_2O_3 particles within the silica porosity, the most interesting results were obtained for the catalysts synthesized following the co-condensation route. Larger iron oxide clusters embedded in the mesoporous silica matrix and coupled to dispersed iron species incorporated in the silica walls proved more efficient as active sites in Fenton catalysis, especially for a long duration catalytic conversion of pollutants such as phenol with hydrogen peroxide.

Acknowledgements

X.L. gratefully acknowledges the Chinese Science Council for a 1-year research grant (no. 2007101600) at the University of Poitiers, France.

R. Palacio, M. Bonne and E. Guélou are sincerely acknowledged for their efficient technical help.

References

[1] M.S. Bahorsky, Textiles, Water Environ. Res. 69 (1997) 658–664.
[2] D.K. Cha, J.S. Song, D. Sarr, B.J. Kim, Hazardous waste treatment technologies, Water. Environ. Res. 68 (1996) 575.
[3] S.F. Kang, C.H. Liao, M.C. Chen, Pre-oxidation and coagulation of textile wastewater by the Fenton process, Chemosphere 46 (2002) 923.
[4] J.A. Theruvathu, C.T. Aravindakumar, R. Flyunt, J.V. Sonntag, C.V. Sonntag, Fenton chemistry of 1,3-dimethyluracil, J. Am. Chem. Soc. 123 (2001) 9007–9014.
[5] B.D. Lee, M. Hosomi, Fenton oxidation of ethanol-washed distillation-concentrated benzo(a)pyrene: reaction product identification and biodegradability, Water Res. 35 (2001) 2314–2319.
[6] W. Gernjak, M. Fuerhacker, P. Fernandez-Ibanez, J. Blanco, S. Malato, Solar photo-Fenton treatment process parameters and process control, Appl. Catal. B: Environ. 64 (2006) 121–130.
[7] L.A. Perez-Estrada, S. Malato, W. Gernjak, A. Aguera, M.E. Thurman, I. Ferrer, A.R. Fernandez-Alba, Photo-Fenton degradation of diclofenac: identification of main intermediates and degradation pathway, Environ. Sci. Technol. 39 (2005) 8300–8306.
[8] A. Coelho, A.V. Castro, M. Dezotti, G.L. Sant Anna Jr., Treatment of petroleum refinery sourwater by advanced oxidation processes, J. Hazard. Mater. B137 (2006) 178–184.
[9] J.M. Monteagudo, A. Duran, C. Lopez-Almodovar, Treatment of petroleum refinery sourwater by advanced oxidation processes, Appl. Catal. B: Environ. 83 (2008) 46–55.
[10] H. Zhang, J.H. Zhang, C.Y. Zhang, F. Liu, D.B. Zhang, Degradation of C.I. acid orange 7 by the advanced Fenton process in combination with ultrasonic irradiation, Ultrason. Sonochem. 16 (2009) 325–330.
[11] F. Ay, E.C. Catalkaya, F. Kargi, A statistical experiment design approach for advanced oxidation of Direct Red azo-dye by photo-Fenton treatment, J. Hazard. Mater. 162 (2009) 230–236.
[12] W. Gernjk, T. Krutzler, A. Glaser, S. Malato, J. Caceres, R. Bauer, A.R. Fernandez-Alba, Photo-Fenton treatment of water containing natural phenolic pollutants, Chemosphere 50 (2003) 71–78.
[13] F. Larachi, S. Levesque, A. Sayari, Wet oxidation of acetic acid by H_2O_2 catalyzed by transition metal-exchanged NaY zeolites, J. Chem. Technol. Biotechnol. 73 (1998) 127–130.
[14] S. Valange, Z. Gabelica, M. Abdellaoui, J.M. Clacens, J. Barrault, Synthesis of copper bearing MFI zeolites and their activity in wet peroxide oxidation of phenol, Micropor. Mesopor. Mater. 30 (1999) 177–185.
[15] G. Centi, S. Perathoner, T. Torre, M.G. Verduna, Catalytic wet oxidation with H_2O_2 of carboxylic acids on homogeneous and heterogeneous Fenton-type catalysts, Catal. Today 55 (2000) 61–69.
[16] G. Centi, S. Perathoner, G. Romeo, Fe/MFI as a new heterogeneous Fenton-type catalyst in the treatment of wastewater from agroindustrial processes, Stud. Surf. Sci. Catal. 135 (2001) 181.
[17] J.A. Melero, G. Calleja, F. Martínez, R. Molina, K. Lázár, Crystallization mechanism of Fe-MFI from wetness impregnated Fe_2O_3–SiO_2 amorphous xerogels: role of iron species in Fenton-like processes, Micropor. Mesopor. Mater. 74 (2004) 11–21.
[18] M.B. Kasiri, H. Aleboyeh, A. Aleboyeh, Degradation of acid blue 74 using Fe-ZSM5 zeolite as a heterogeneous photo-Fenton catalyst, Appl. Catal. B: Environ. 84 (2008) 9–15.
[19] M. Tekbas, H.C. Yatmaz, N. Bektas, Heterogeneous photo-Fenton oxidation of reactive azo dye solutions using iron exchanged zeolite as a catalyst, Micropor. Mesopor. Mater. 115 (2008) 594–602.
[20] V.K. Maduna, K. Andrea, T. Vesna, Z. Stanka, Characterization and activity of Cu/ZSM5 catalysts for the oxidation of phenol with hydrogen peroxide, Chem. Eng. J. 31 (2008) 398–403.
[21] A. Chen, X. Ma, H. Sun, Decolorization of KN-R catalyzed by Fe-containing Y and ZSM-5 zeolites, J. Hazard. Mater. 156 (2008) 568–575.
[22] S. Parra, V. Nadtotechenko, P. Albers, J. Kiwi, Discoloration of azo-dyes at biocompatible pH-values through an Fe–histidine complex immobilized on nafion via fenton-like processes, J. Phys. Chem. B 108 (2004) 4439.
[23] H. Sueh, Y.H. Huang, C.Y. Chen, Novel activated alumina-supported iron oxide-composite as a heterogeneous catalyst for photooxidative degradation of reactive black 5, J. Hazard. Mater. B 129 (2006) 228–233.
[24] M. Inbasekaran, S. Meenakshisundaram, Photoassisted Fenton mineralisation of Acid Violet 7 by heterogeneous Fe(III)–Al_2O_3 catalyst, Catal. Commun. (2007) 981–986.
[25] M. Inbasekaran, S. Meenakshisundaram, Highly solar active Fe(III) immobilised alumina for the degradation of Acid Violet 7, Sol. Energy. Mater. Sol. C. 92 (2008) 857–863.
[26] J.A. Zazo, J.A. Casas, A.F. Mohedano, J.J. Rodriguez, Catalytic wet peroxide oxidation of phenol with a Fe/active carbon catalyst, Appl. Catal. B 65 (2006) 261–268.
[27] J.H. Ramirez, F.J. Maldonado-Hodar, A.F. Perez-Cadenas, C. Moreno-Castilla, C.A. Costa, L.M. Madeira, Azo-dye Orange II degradation by heterogeneous Fenton-like reaction using carbon-Fe catalysts, Appl. Catal. B 75 (2007) 312–323.
[28] A. Rey, M. Faraldos, J.A. Casas, J.A. Zazo, A. Bahamonde, J.J. and, Rodríguez, Catalytic wet peroxide oxidation of phenol over Fe/AC catalysts: influence of iron precursor and activated carbon surface, Appl. Catal. B 86 (2009) 69–77.
[29] R.M. Liou, S.H. Chen, M.Y. Hung, C.S. Hsu, J.Y. Lai, Fe (III) supported on resin as effective catalyst for the heterogeneous oxidation of phenol in aqueous solution, Chemosphere 59 (2005) 117–125.
[30] J. Fernandez, M.R. Dhananjeyan, J. Kiwi, Evidence for Fenton photoassisted processes mediated by encapsulated Fe ions at biocompatible pH values, J. Phys. Chem. B 104 (2000) 5298–5301.
[31] J. Barrault, M. Abdellaoui, C. Bouchoule, A. Majesté, J.M. Tatibouët, A. Louloudi, N. Papayannakos, N.H. Gangas, Catalytic wet peroxide oxidation over mixed (Al–Fe) pillared clays, Appl. Catal. B 27 (2000) 225.
[32] E. Guélou, J. Barrault, J. Fournier, J.-M. Tatibouët, Active iron species in the catalytic wet peroxide oxidation of phenol over pillared clays containing iron, Appl. Catal. B 44 (2003) 1–8.
[33] S. Perathoner, G. Centi, Wet hydrogen peroxide catalytic oxidation (WHPCO) of organic waste in agro-food and industrial streams, Top. Catal. 33 (2005) 207–224.
[34] C.B. Molina, J.A. Casas, J.A. Zazo, J.J. Rodríguez, A comparison of Al-Fe and Zr-Fe pillared clays for catalytic wet peroxide oxidation, Chem. Eng. J. 118 (2006) 29–35.
[35] G. Girolamo, S. Perathoner, G. Centi, S. De Rosa, T. Granato, A. Katovic, A. Siciliano, A. Tagarelli, F. Tripicchio, Wet hydrogen peroxide catalytic oxidation of olive oil mill wastewaters using Cu-zeolite and Cu-pillared clay catalysts, Catal. Today 124 (2007) 240–246.
[36] S. Caudo, G. Centi, C. Genovese, S. Perathoner, Copper- and iron-pillared clay catalysts for the WHPCO of model and real wastewater streams from olive oil milling production, Appl. Catal. B 70 (2007) 437–446.
[37] N.R. Sanabria, M.A. Centeno, R. Molina, S. Moreno, Pillared clays with Al–Fe and Al–Ce–Fe in concentrated medium: synthesis and catalytic activity, Appl. Catal. A 356 (2009) 243–249.
[38] J.L. Sotelo, G. Ovejero, F. Martínez, J.A. Melero, A. Milieni, Catalytic wet peroxide oxidation of phenolic solutions over a $LaTi_{1-x}Cu_xO_3$ perovskite catalyst, Appl. Catal. A 47 (2004) 281–294.
[39] A. Xu, M. Yang, R. Qiao, H. Du, C. Sun, Activity and leaching features of zinc-aluminum ferrites in catalytic wet oxidation of phenol, J. Hazard. Mater. 147 (2007) 449–456.
[40] J. Faye, E. Guélou, J. Barrault, J.M. Tatibouët, S. Valange, $LaFeO_3$ perovskite as new and performant catalyst for the wet peroxide oxidation of organic pollutants in ambient conditions, Top. Catal. 52 (2009) 1211–1219.
[41] F. Martinez, Y. Jhan, G. Stucky, J.L. Sotelo, G. Ovejero, J.A. Melero, Synthesis and characterisation of iron-containing SBA-15 mesoporous silica, Stud. Surf. Sci. Catal. 142 (2002) 1109–1116.
[42] K. Lázár, G. Calleja, J.A. Melero, F. Martinez, R. Molina, Influence of synthesis routes on the state of Fe-species in SBA-15 mesoporous materials, Stud. Surf. Sci. Catal. 154 (2004) 805–812.
[43] G. Calleja, J.A. Melero, F. Martinez, R. Molina, Activity and resistance of iron-containing amorphous, zeolitic and mesostructured materials for wet peroxide oxidation of phenol, Water Res. 39 (2005) 1741–1750.
[44] F. Martinez, G. Calleja, J.A. Melero, R. Molina, Heterogeneous photo-Fenton degradation of phenolic aqueous solutions over iron-containing SBA-15 catalyst, Appl. Catal. B 60 (2005) 181–190.
[45] J.A. Melero, G. Calleja, F. Martinez, R. Molina, Nanocomposite of crystalline Fe_2O_3 and CuO particles and mesostructured SBA-15 silica as an active catalyst for wet peroxide oxidation processes, Catal. Commun. 7 (2006) 478–483.
[46] J.A. Melero, G. Calleja, F. Martínez, R. Molina, M.I. Pariente, Nanocomposite Fe_2O_3/SBA-15: an efficient and stable catalyst for thecatalytic wet peroxidation of phenolic aqueous solutions, Chem. Eng. J. 131 (2007) 245–246.
[47] R. Pechini, US Patent 3,330,697 (1967).

[48] M. Bonne, N. Bion, F. Pailloux, S. Valange, S. Royer, J.-M. Tatibouët, D. Duprez, Improved oxygen mobility in nanosized mixed-oxide particles synthesized using a simple nanocasting route, Chem. Commun. (2008) 4504.
[49] J.-M. Tatibouët, E. Guélou, J. Fournier, Catalytic oxidation of phenol by hydrogen peroxide over a pillared clay containing iron. Active species and pH effect, Top. Catal. 33 (2005) 225–232.
[50] M. Abdellaoui, PhD Thesis, University of Poitiers, France, 1999.
[51] S. Valange, A. Charmot, J. Barrault, A. Louati, Z. Gabelica, Insertion of Fe_2O_3 nanoparticles in SBA-15 mesopores and evaluation of their textural and redox characteristics, Stud. Surf. Sci. Catal. 170A (2007) 531–538.
[52] Z. Gabelica, A. Charmot, R. Vataj, R. Soulimane, J. Barrault, S. Valange, Thermal degradation of iron chelate complexes adsorbed on mesoporous silica and alumina, J. Thermal Anal. Calorim. 95 (2009) 445–454.